Determination of the distance between $Y_Z^{ox\bullet}$ and $Q_A^{-\bullet}$ in photosystem II by pulsed EPR spectroscopy on light-induced radical pairs

Stephan G. Zech, Jens Kurreck, Gernot Renger, Wolfgang Lubitz, Robert Bittl*

Max-Volmer-Institut für Biophysikalische Chemie und Biochemie, Technische Universität Berlin, Straße des 17. Juni 135, 10623 Berlin, Germany

Received 11 November 1998

Abstract Out-of-phase electron spin echo envelope modulation (ESEEM) spectroscopy was used to determine the distances within two consecutive radical pair states initiated by a laser flash in photosystem II membrane fragments at pH 11. The distance between the spin density centers of the primary electron donor cation radical, $P_{680}^{+\bullet}$, and the reduced plastoquinone acceptor, $Q_A^{-\bullet}$, has been found to be 27.7 ± 0.7 Å in agreement with previous results. Near room temperature and at high pH, $P_{680}^{+\bullet}$ is reduced by Y_Z, a redox active tyrosine residue, on a submicrosecond timescale. As a consequence, the subsequent radical pair state, $Y_Z^{ox\bullet}Q_A^{-\bullet}$, could be investigated after almost complete reduction of $P_{680}^{+\bullet}$ by Y_Z. The determined dipolar electronic spin-spin coupling within the radical pair $Y_Z^{ox\bullet}Q_A^{-\bullet}$ corresponds to a distance of 34 ± 1 Å between the two molecules.

Key words: Radical pair; Cofactor distance; Photosystem II; Pulsed electron paramagnetic resonance

1. Introduction

The key step of photosynthetic energy conversion, the light-induced electron transfer (ET), occurs in membrane-bound protein-cofactor complexes. Knowledge of the structure of these reaction centers (RCs) is a prerequisite for a detailed understanding of photosynthesis. The architecture of oxygen evolving photosystem II (PS II) has so far not been obtained from crystallographic studies. Only for a core of PS II, lacking the water oxidizing complex, a structural model has been published based on electron crystallography at 8 Å resolution on two-dimensional crystals [1,2]. PS II single crystals which diffract X-rays to about 5 Å have been obtained only recently [3].

A different approach of building a structural model of the PS II core including the electron transfer chain is based on structural and functional homologies between the D1 and D2 protein subunits of PS II and the L and M subunits of the reaction centers of purple bacteria. Starting from the well resolved structure of the purple bacterial RC (bRCs) and using molecular modeling techniques several models of the PS II core complex have been presented (see [4–6] and references therein). However, especially for the donor side of PS II functional differences to bRCs exist. The primary donor, P_{680}, has an unusual redox potential and a redox active tyrosine residue acts as an intermediary electron carrier between the water oxidizing complex and $P_{680}^{+\bullet}$. These specific properties are expected to be influenced by structural differences between bRCs and PS II. Therefore, independent information is clearly necessary to verify the validity of the PS II structures obtained from molecular modeling.

Time-resolved EPR spectroscopy has already provided such information, in particular on distances between redox active cofactors in PS II (see e.g. [7,8] and references therein). The most precise long-range distance measurements by EPR make use of the out-of-phase electron spin echo envelope modulation (ESEEM) induced by the dipolar electronic spin-spin coupling in light-induced radical pair states [9,10]. This technique yields accurate distances as shown by earlier experiments on bRCs [11,12] with the respective distances known from the ground state X-ray structure. For photosystem I of oxygenic photosynthesis structural data obtained by out-of-phase ESEEM [13] have been used as a basis for the assignment of the electron acceptor A_1, a phylloquinone, to an electron density in X-ray crystallography [14].

The out-of-phase ESEEM technique has also been applied to PS II and yielded the distance between $P_{680}^{+\bullet}$ and $Q_A^{-\bullet}$ [9,10]. Knowledge of this distance is important for the following reasons. (i) It is a test criterion for the PS II model structures and has already been used for this purpose [6]. (ii) More importantly, the distance from $P_{680}^{+\bullet}$ to other redox active components in PS II will be helpful for the assignment of the oxidized species $P_{680}^{+\bullet}$ to one or more of the chlorophyll molecules bound by the D1 and D2 protein subunits. This assignment cannot be obtained on the basis of crystallographic or modeling studies alone.

In the present study, we concentrate on the distance between the redox active tyrosine residue Y_Z in D1 and the primary quinone acceptor Q_A. This will extend the spectroscopically determined structural data base for PS II. Furthermore, the precise distance between Y_Z and Q_A provides an anchor point for assignments of individual amino acids even in an electron density map of relatively low resolution.

To obtain the distance from $Y_Z^{ox\bullet}$ to $Q_A^{-\bullet}$ we used the acceleration of the electron transfer from Y_Z to $P_{680}^{+\bullet}$ with increasing pH in PS II particles deprived of the water oxidizing complex. The decreased lifetime of the state $P_{680}^{+\bullet}Q_A^{-\bullet}$ results in a larger error margin of the distance determination for this state as compared to [9]. However, it allows a rather precise evaluation of the distance between $Y_Z^{ox\bullet}$ and $Q_A^{-\bullet}$.

2. Materials and methods

PS II membrane fragments were prepared from market spinach

*Corresponding author. Fax: (49) (30) 31421122.
E-mail: bittl@chem.tu-berlin.de

Abbreviations: bRC, bacterial reaction center; CAPS, 3-[cyclohexylamino]-1-propane-sulfonic acid; EPR, electron paramagnetic resonance; ESEEM, electron spin echo envelope modulation; ET, electron transfer; mw, microwave; P_{680}, primary donor of PS II; Q_A, primary quinone electron acceptor in PS II and bRCs; A_1, primary quinone electron acceptor in PS I; RP, radical pair; SFT, sine Fourier transform; Y_Z, redox active tyrosine residue of polypeptide D1

0014-5793/99/$19.00
PII: S0014-5793(98)01628-7

according to [15] with some modifications as described previously [16]. The EPR measurements were performed on membrane fragments diluted in a buffer at pH 11. Therefore, the samples were washed twice in a buffer containing 50 mM CAPS/NaOH (pH 11), 10 mM NaCl and 1 mM NaEDTA and diluted to a chlorophyll concentration of about 7 mg/ml. The total sample volume was approximately 6 ml.

The very high pH of 11 was used for two reasons. (i) At higher pH values, the ET from Y_Z to $P_{680}^{+\bullet}$ becomes faster (<1 μs) [17–19]. (ii) The out-of-phase ESEEM technique requires the excitation of the whole spin-polarized EPR spectrum, i.e. both spins (on donor and acceptor) have to be excited simultaneously by the microwave (mw) pulses. For this purpose, a decoupling of the $Q_A^{-\bullet}$ molecule from the paramagnetic non-heme, high spin Fe^{2+} ion is necessary. In the case of PS II, non-heme iron-depleted (Fe-depleted) or cyanide-treated samples are widely used for EPR studies of the uncoupled $Q_A^{-\bullet}$. Recently, a decoupling at pH 11 values has been reported [20]. The reason for this decoupling is not established yet. We used this decoupling method since the sample preparation is highly simplified by omission of the preparation step for removing the non-heme iron center. For a detailed analysis, however, it has to be kept in mind that the micro-environment of $Q_A^{-\bullet}$ is not identical in both sample types (see [21] and discussion below).

The pulsed EPR measurements were performed near room temperature using a continuous flow system as described earlier [9]. In this study we used a $h\nu$-t-$\zeta/2$-τ-ζ pulse sequence with pulse lengths of 8 ns and 16 ns, respectively and an increment of the pulse separation τ of 8 ns. A microwave power of nominally 1 kW has been used to achieve maximum echo intensity at $\zeta \approx 130°$. Evaluation of the spin-spin coupling parameters from Fourier transformed ESEEM traces was performed as described previously [9,11].

3. Results

Fig. 1 (top) shows the scheme of the experimental pulse sequence. After a delay time t following the initial laser pulse, a 2 mw pulse sequence is applied. The resulting out-of-phase electron spin echo is detected at time $T \approx \tau$ after the second mw pulse. The echo intensity is depicted in Fig. 1A–C as function of the pulse separation τ for different delay times t. Trace A corresponds to $t = 50$ ns. During the first 400 ns in τ, the observed modulation pattern is very similar to that found for Fe-depleted PS II particles with blocked ET from Y_Z to $P_{680}^{+\bullet}$ [9], except for a decreased signal-to-noise ratio. The observed similarities can be understood on the basis of the ET times. The RP state $P_{680}^{+\bullet}Q_A^{-\bullet}$ is formed within 350 ps after the laser flash (see e.g. [22,23]). Since the ET from Y_Z to $P_{680}^{+\bullet}$ takes place on a timescale of several hundred nanoseconds at high pH (see e.g. [18,19]) the signal observed at $t = 50$ ns and $\tau < 400$ ns is dominated by the RP state $P_{680}^{+\bullet}Q_A^{-\bullet}$.

With increasing pulse spacing τ a faster damping of the echo modulation than previously found for samples at pH 6.5 and 9.0 [9] is observed. This indicates a relatively short lifetime of the RP state $P_{680}^{+\bullet}Q_A^{-\bullet}$ due to the reduction of $P_{680}^{+\bullet}$ by Y_Z and leads to the conclusion that the ET from Y_Z to $P_{680}^{+\bullet}$ at pH 11 is faster than in our previous study [9]. This is in accordance with optical studies [18,19].

Fig. 1B shows the observed time trace for $t = 1$ μs. The significant decrease of the modulation frequency indicates an increasing contribution of the RP state $Y_Z^{ox\bullet}Q_A^{-\bullet}$ which has a considerable smaller spin-spin coupling than that in $P_{680}^{+\bullet}Q_A^{-\bullet}$. However, at times $\tau < 300$ ns, a small amount of the RP state $P_{680}^{+\bullet}Q_A^{-\bullet}$ is still present, showing that $P_{680}^{+\bullet}$ is incompletely reduced at this time. Hence, a quantitative analysis of the observed echo modulation in Fig. 1B has to account for the superposition of two consecutive RP states [24].

The faster modulation that is still present at $t = 1$ μs is no longer visible at a delay time of $t = 2$ μs as shown in Fig. 1C.

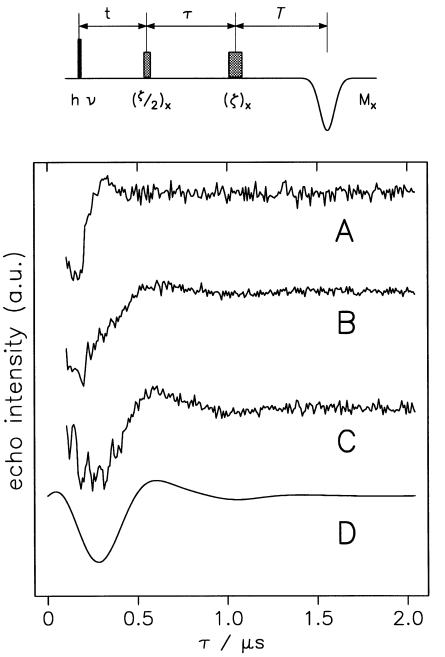

Fig. 1. Out-of-phase electron spin echo modulation from PS II membrane fragments at pH 11 near room temperature using the pulse scheme shown at the top. The three experimental spectra (A–C) correspond to delay times between the laser flash ($h\nu$) and the first mw pulse of $t = 50$ ns (A), 1 μs (B) and 2 μs (C). Trace D shows the numerical simulation of the out-of-phase modulation according to the CCRP theory with spin-spin coupling parameters $D = -71$ μT and $J = 1$ μT corresponding to a distance between $Y_Z^{ox\bullet}$ and $Q_A^{-\bullet}$ of 34 Å.

A clear disadvantage of this large delay time is the drastically reduced echo intensity due to spin-lattice relaxation processes, giving rise to a smaller signal-to-noise ratio. Improvement of the signal-to-noise ratio by further accumulation of the echo modulation was not possible due to sample degradation as a result of the repetitive laser excitation.

Besides the relatively slow modulation with a period of about 900 ns, which is attributed to the electron-electron spin-spin interaction, a modulation with much higher frequency is visible in Fig. 1C, especially for $\tau < 500$ ns. These faster modulations have frequencies between 14 and 16 MHz as revealed from Fourier transforms (not shown) and are attributed to anisotropic electron-nuclear hyperfine interactions within $Y_Z^{ox\bullet}$. Since we are only interested in electron-electron spin interactions in this study, these higher frequency oscillations are not evaluated in detail.

According to the theoretical analysis of out-of-phase ESEEM for a system undergoing secondary electron transfer [24], the ESEEM in the secondary radical pair can be well described without consideration of the primary pair for delay times t much longer than the electron transfer time constant. The slow echo modulation observed in Fig. 1C agrees well with a numerical simulation according to the CCRP model for *one* RP state (Fig. 1D). This demonstrates that $P_{680}^{+\bullet}$ has been almost completely reduced by Y_Z prior to the first mw pulse and, hence, the echo modulation is dominated by the RP state $Y_Z^{ox\bullet}Q_A^{-\bullet}$ (see below).

Fig. 2 shows the Fourier transformed echo modulations of Fig. 1 after reconstruction of the signal within the spectrometer deadtime as described previously [11]. Spectrum A is in

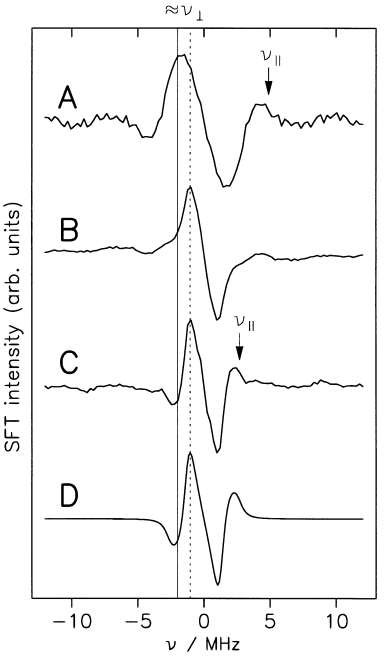

Fig. 2. Sine Fourier transforms of the echo modulations shown in Fig. 1. The solid and the dotted vertical lines indicate the dominant modulation frequency (approximately $\nu_\perp$) for the RP states $P_{680}^{+\bullet}Q_A^{-\bullet}$ (A) and $Y_Z^{ox\bullet}Q_A^{-\bullet}$ (C), respectively.

qualitative agreement with the spectrum obtained for Fe-depleted PS II particles measured at pH 9 [9] for the same delay time t. The broadening of the dominant modulation frequency observed in the range $1.7 < \nu < 2.1$ MHz is now more pronounced than at pH 9 [9]. This line broadening is a result of the fast damping of the echo modulation due to the limited lifetime of $P_{680}^{+\bullet}Q_A^{-\bullet}$ [11,24]. The same effect is responsible for the apparent shift of the dominant peak to lower frequencies compared with photoinhibited samples [9]. A numerical simulation of the SFT of Fig. 2A reveals a dipolar coupling of $D = -(131 \pm 10)$ μT, which is (within error) in agreement with the value found previously for the photo-inhibited and Fe-depleted PS II sample [9]. The dipolar coupling corresponds to a distance of 27.7 ± 0.7 Å between the spin density centers on the respective cofactors. The larger error margin given here is the result of the faster damping of the echo signal and the corresponding line broadening of the SFT.

At longer delay times, the dominant modulation frequency peaks (approximately $\nu_\perp$, see e.g. [11]) narrow and shift their maxima to $|\nu_{max}| \approx 1.1$ MHz as visible in traces A–C in Fig. 2. Furthermore, the frequency component attributed to $\nu_\parallel$ [11,12] shifts from $|\nu_\parallel| \approx 4.9$ MHz in Fig. 2A,B to $|\nu_\parallel| \approx 2.7$ MHz in Fig. 2C. A comparison with numerical simulations given in [24] shows that the spectrum obtained at a delay time of $t = 1$ μs (Fig. 2B) reflects a superposition of the RP states $P_{680}^{+\bullet}Q_A^{-\bullet}$ and $Y_Z^{ox\bullet}Q_A^{-\bullet}$. The same conclusion has been drawn from the qualitative interpretation of the time traces (see above).

In contrast, the spectrum shown in Fig. 2C with $t = 2$ μs is almost exclusively governed by the RP state $Y_Z^{ox\bullet}Q_A^{-\bullet}$ and enables a direct determination of the spin-spin coupling in this state. Fig. 2D shows the numerical simulation considering only the state $Y_Z^{ox\bullet}Q_A^{-\bullet}$. The best agreement with the experimental spectrum of Fig. 2C is obtained for the dipolar spin-spin coupling parameter $D = -71 \pm 6$ μT. For the exchange coupling J an upper limit of about 1 μT can be given. In a simple point-dipole approximation, D yields a distance between the spin density centers on $Y_Z^{ox\bullet}$ and $Q_A^{-\bullet}$ of 34 ± 1 Å. The relatively large error for this distance is the result of (i) the limited signal-to-noise ratio of the obtained echo modulation pattern and the corresponding SFT, and (ii) the smaller absolute value for D, giving rise to a larger relative error of the distance.

4. Discussion and conclusion

In a preceding paper we determined the distance between the oxidized primary donor, $P_{680}^{+\bullet}$, and the reduced acceptor quinone, $Q_A^{-\bullet}$, by application of out-of-phase ESEEM spectroscopy. A distance of 27.4 ± 0.3 Å between the centers of the spin densities on the respective molecules has been found in Fe-depleted PS II preparations measured under physiological conditions, i.e. at room temperature and pH 6.5 [9]. Independently, Hara et al. [10] obtained an almost identical distance of 27.2 ± 1 Å by applying the same experimental method. These authors worked at low temperature (80 K) and used different types of PS II samples (Zn-substituted or cyanide-treated core complexes and quinone reconstituted D1-D2-cyt b_{559} complexes).

At ambient temperatures and pH 9, an ET from Y_Z to $P_{680}^{+\bullet}$ occurs on a microsecond time scale. This enabled the detection of two different radical pair states, $P_{680}^{+\bullet}Q_A^{-\bullet}$ and $Y_Z^{ox\bullet}Q_A^{-\bullet}$, in the same experiment [9]. From the dependence of the major modulation frequency observed in the Fourier transformed time traces, a lower limit for the distance between $Y_Z^{ox\bullet}$ and $Q_A^{-\bullet}$ of 32 Å was obtained for the Fe-depleted samples [9]. The fast spin-lattice relaxation at room temperature prevented an unambiguous determination of the distance between $Y_Z^{ox\bullet}$ and $Q_A^{-\bullet}$ at longer delay times t where $P_{680}^{+\bullet}$ is completely reduced. At shorter times, the recorded spectra always represented the superposition of the RP state $P_{680}^{+\bullet}Q_A^{-\bullet}$ and $Y_Z^{ox\bullet}Q_A^{-\bullet}$ [9].

In order to account for such a superposition of two consecutive RPs, a theoretical treatment for the out-of-phase ESEEM in reacting systems has been developed [24]. The numerical simulations showed that a change in the orientation of the dipolar axis, as expected for a sequence of RPs, does not considerably influence the Fourier transformed echo modulations. A determination of the principal values of the dipolar coupling tensors is, therefore, possible for a superposition of two sequential RPs, even when the relative orientation of the dipolar axes and the ET rate are not exactly known. Using the experimental data for the Fe-depleted preparation at pH 9 [9], a distance between $Y_Z^{ox\bullet}$ and $Q_A^{-\bullet}$ of 35 ± 3 Å has been estimated [24]. In the present study, however, we chose a high pH value to accelerate the reduction of $P_{680}^{+\bullet}$ and hence to determine the distance between $Y_Z^{ox\bullet}$ and $Q_A^{-\bullet}$ of 34 ± 1 Å with higher accuracy.

For comparison with data gathered from other methods it should be kept in mind that the magnetic decoupling of $Q_A^{-\bullet}$ from the non-heme Fe^{2+} requires relatively harsh biochemical procedures (see above) which may alter the environment of Q_A. ESEEM experiments on chemically generated $Q_A^{-\bullet}$ which are sensitive to electron-nuclear hyperfine couplings have shown that the magnetic coupling between the $Q_A^{-\bullet}$ and an imidazole ring attributed to a histidine residue [25] is lost in cyanide-treated samples [26–28]. On the other hand, this interaction is present in Fe-depleted [28] preparations as well as

in samples at high pH [20]. Recent FTIR investigations [21] have shown that the micro-environment of $Q_A^{-\bullet}$ in Fe-depleted samples is virtually identical to that of native samples. In cyanide- or high pH-treated preparations an H-bond between the carbonyl oxygen atom of Q_A and a histidine residue in its environment is lost. The observed differences are clearly more pronounced in cyanide-treated samples [21].

The determination of an almost identical distance within the RP state $P_{680}^{+\bullet}Q_A^{-\bullet}$ and the agreement between the distance within $Y_Z^{ox\bullet}Q_A^{-\bullet}$ measured at pH 11 and the estimates derived previously for samples at pH 9 (see above and [9,24]) indicate that the cofactor distances in Fe-depleted samples are almost identical compared to preparations at high pH. The distances between Y_Z and Q_A in a recent molecular modeling study by Xiong et al. [6] are also consistent with the value of 34 Å obtained here.

Finally, the precise distance between $Y_Z^{ox\bullet}$ and $Q_A^{-\bullet}$ determined here will be useful for an assignment of the important amino acid residue Y_Z already in an electron density map of low or intermediate resolution.

Acknowledgements: The authors thank S. Kussin and B. Lange for technical assistance. This work has been supported by Deutsche Forschungsgemeinschaft (SFB 312, TP A2/A4; Schwerpunktprogramm Hochfeld-EPR) and Fonds der Chemischen Industrie (to W.L. and G.R.).

References

[1] Morris, E.P., Hankamer, B., Zheleva, D., Friso, G. and Barber, J. (1997) Structure 5, 837.
[2] Rhee, K.-H., Morris, E.P., Barber, J. and Kühlbrandt, W. (1998) Nature 396, 283.
[3] Zouni, A., Lüneberg, C., Fromme, P., Schubert, W.D., Saenger, W. and Witt, H.T. (1998) in: Photosynthesis: Mechanisms and Effects (Garab, G., Ed.), Kluwer Academic, Dordrecht, in press.
[4] Ruffle, S.V., Donnelly, D., Blundell, T.L. and Nugent, J.H.A. (1992) Photosynth. Res. 34, 287.
[5] Svensson, B., Etchebest, C., Tuffery, P., van Kan, P., Smith, J. and Styring, S. (1996) Biochemistry 35, 14486.
[6] Xiong, J., Subramaniam, S. and Govindjee (1998) Photosynth. Res. 56, 229.
[7] Koulougliotis, D., Schweitzer, R.H. and Brudwig, G.W. (1997) Biochemistry 36, 9735.
[8] Shigemori, K., Hara, H., Kawamori, A. and Akabori, K. (1998) Biochim. Biophys. Acta 1363, 187.
[9] Zech, S.G., Kurreck, J., Eckert, H.-J., Renger, G., Lubitz, W. and Bittl, R. (1997) FEBS Lett. 414, 454.
[10] Hara, H., Dzuba, S.A., Kawamori, A., Akabori, K., Tomo, T., Satoh, K., Iwaki, M. and Itoh, S. (1997) Biochim. Biophys. Acta 1322, 77.
[11] Bittl, R. and Zech, S.G. (1997) J. Phys. Chem. B 101, 1429.
[12] Dzuba, S.A., Gast, P. and Hoff, A.J. (1997) Chem. Phys. Lett. 268, 273.
[13] Bittl, R., Zech, S.G., Fromme, P., Witt, H.T. and Lubitz, W. (1997) Biochemistry 36, 12001.
[14] Schubert, W.-D., Klukas, O., Krauß, N., Saenger, W., Fromme, P. and Witt, H.T. (1997) J. Mol. Biol. 272, 741.
[15] Berthold, D.A., Babcock, G. and Yocum, C.F. (1981) FEBS Lett. 134, 231.
[16] Völker, M., Ono, T., Inoue, Y. and Renger, G. (1985) Biochim. Biophys. Acta 806, 25.
[17] Conjeaud, H. and Mathis, P. (1980) Biochim. Biophys. Acta 590, 353.
[18] Schlodder, E. and Meyer, B. (1987) Biochim. Biophys. Acta 890, 23.
[19] Ahlbrick, R., Haumann, M., Cherepanov, D., Bögershausen, O., Mulkidjanian, A. and Junge, W. (1998) Biochemistry 37, 1131.
[20] Deligiannakis, Y., Jegerschöld, C. and Rutherford, A.W. (1997) Chem. Phys. Lett. 270, 564.
[21] Nogouchi, T., Kurreck, J., Inoue, Y. and Renger, G. (1998) Biochemistry (submitted).
[22] Nuijs, A.M., van Gorkom, H.J., Plijter, J.J. and Duysens, L.N.M. (1986) Biochim. Biophys. Acta 848, 167.
[23] Eckert, H.-J., Wiese, N., Bernarding, J., Eichler, H.-J. and Renger, G. (1988) FEBS Lett. 240, 153.
[24] Jeschke, G. and Bittl, R. (1998) Chem. Phys. Lett. 294, 323.
[25] Astashkin, A.V., Kawamori, A., Kodera, Y., Kuroiwa, S. and Akabori, K. (1995) J. Chem. Phys. 102, 5583.
[26] Deligiannakis, Y., Boussac, A. and Rutherford, A.W. (1995) Biochemistry 34, 16030.
[27] MacMillan, F., Kurreck, J., Adir, N., Lendzian, F., Käß, H., Reifarth, F., Renger, G. and Lubitz, W. (1995) in: Photosynthesis: from Light to Biosphere (Mathis, P., Ed.), Vol. I, pp. 659–662, Kluwer Academic, Dordrecht.
[28] Renger, G., Kurreck, J., Haag, E., Reifarth, F., Bergmann, A., Parak, F., Garbers, A., MacMillan, F., Lendzian, F. and Lubitz, W. (1997) in: Bioinorganic Chemistry (Trautwein, A.X., Ed.), pp. 260–277, Wiley-VCH, Weinheim.